Behavior of Hollow-Core Steel-Concrete-Steel Columns Subjected to Torsion Loading

Sujith Anumolu[1]; Omar I. Abdelkarim, S.M.ASCE[2]; and Mohamed A. ElGawady, Ph.D., M.ASCE[3]

Abstract: The torsional behavior of hollow-core steel-concrete-steel (HC-SCS) columns is presented using finite-element (FE) and analytical approaches. The HC-SCS columns consist of a concrete shell sandwiched between two steel tubes. Software was used to develop a three-dimensional model of an HC-SCS column that was subjected to torsional loading. The FE results were validated against the experimental results collected from six HC-SCS columns tested under pure torsion. The average error from the FE analysis was 4.8%, compared with experimental results, when predicting the column's torsion strength. The study revealed that the interaction between the steel tube's stiffness and concrete shell's thickness controls the behavior of the column. A parametric study was conducted to further analyze each parameter affecting the column's torsion behavior. The parametric analysis concluded that the torsional behavior of the column mainly depends on the outer steel tube's properties and the thickness of the concrete shell. A simplified equation was developed to predict the torsion strength of the member using a direct method of stress analysis. The proposed equation predicted the members' torsion strength with an accuracy greater than 90%. **DOI: [10.1061/(ASCE)BE.1943-5592.0000923](#).** © *2016 American Society of Civil Engineers.*

Author keywords: Finite-element (FE) modeling; Steel-concrete-steel columns (SCS); Bridge column; *LS-DYNA*.

Introduction

Researchers have recently focused on developing new cost-effective design and construction methods for accelerating bridge construction (ABC), which leads to improved site constructability and work zone safety as well as a reduction in traffic disruptions and lifecycle costs (Dawood et al. 2011, 2014; Abdelkarim et al. 2015). One approach to accelerate the construction of bridge columns and shafts, while obtaining a higher seismic performance, is to use concrete-filled steel tubular (CFST) columns that encase the concrete core in a steel tube.

The CFST members possess several benefits over reinforced concrete (RC) or steel members. The steel tube in a CFST column acts as a stay-in-place formwork that provides longitudinal and shear reinforcement to the member and continuous confinement to the concrete core. Furthermore, the concrete core in a CFST column acts as bracing to the steel tube and provides lateral stability, which delays steel tube local buckling. Hence, CFST members displayed superior performance under earthquake ground motions (Bi et al. 2013).

A typical bridge column would sustain 5–10% of its ultimate axial load capacity due to service axial loads (Mondal and Prakash 2015a). The design of bridge columns in seismic regions is typically controlled by the bridge's lateral stiffness demand. Hence, researchers developed a hollow-core CFST system. The system consisted of an inner and outer steel tube and used concrete to fill the space between the two tubes (Wei et al. 1995; Lin and Tsai 2001; Zhao et al. 2002; Tao and Han 2006). The lateral stability provided by the concrete shell to the steel tube enhances the initial stiffness and ductility of the column. The main advantage of hollow-core steel-concrete-steel (HC-SCS) columns is their high strength-to-weight ratio compared with columns with solid cross sections (Han et al. 2006). A lighter weight is crucial for reducing the freight cost in precast construction. Furthermore, reducing the column's weight will reduce the seismic inertial forces in long columns.

A number of investigators recently studied the behavior of HC-SCS columns under different types of loading conditions (Zhao et al. 2010; Elchalakani et al. 2002; Tao et al. 2004; Han et al. 2006; Lu et al. 2010; Dong and Ho 2012; Hassanein et al. 2013; Li et al. 2014). Most of the studies were limited to axial and flexural loadings with different cross sections. These studies depicted that the confinement was active after the concrete shell cracked and dilated. In addition, they reported that the buckling of the steel tubes was significantly delayed because of the lateral support from the concrete. They also found that the influence of the concrete shell's thickness on the ductility of the column was small.

Bridge columns are subjected to torsional loads in curved and skewed bridges during earthquakes. Typically, torsion exists in combination with axial and flexural loads. However, because torsional behavior is complicated, most researchers investigated the performance of bridge columns under pure torsional loads to better understand column behavior (Beck and Kiyomiya 2003; Han et al. 2007; Lee et al. 2009; Nie et al. 2012; Huang et al. 2013). Other researchers investigated the behavior of bridge columns under combined torsional, flexural, and/or axial loads (Belarbi et al. 2008; Prakash and Belarbi 2009; Mullapudi and Ayoub 2012; Ruili et al. 2014; Mondal and Prakash 2015a, b). Most of these torsional studies focused on conventional RC columns or CFST columns.

[1]Graduate Research Assistant, Dept. of Civil, Architectural, and Environmental Engineering, Missouri Univ. of Science and Technology, Rolla, MO 65401. E-mail: sat6f@mst.edu

[2]Ph.D. Candidate, Dept. of Civil, Architectural, and Environmental Engineering, Missouri Univ. of Science and Technology, Rolla, MO 65401. E-mail: oiafgc@mail.mst.edu

[3]Benavides Associate Professor, Dept. of Civil, Architectural, and Environmental Engineering, Missouri Univ. of Science and Technology, Rolla, MO 65401 (corresponding author). E-mail: elgawadym@mst.edu

However, very few studies examined the torsional behavior of HC-SCS columns. Under pure torsion, the RC columns failed because of concrete spalling and transverse reinforcement rupturing at the middle height of the column. However, the confinement of the steel tubes in HC-SCS columns prevented concrete spalling. The confinement of the steel tubes endeavors the torsional load carried by the concrete shell.

Huang et al. (2013) were the first to experimentally investigate the pure torsional behavior of HC-SCS columns. The investigation showed that HC-SCS columns have significant strength, ductility, and energy absorption. The investigation revealed that the concrete shell enhanced the column's ultimate torque by 20%. The researchers reported that the concrete shell cracked at 45° to the axis and maintained its shape. The concrete shell was well bonded with the outer steel tube and no sliding was observed. They reported that the outer steel tube's strength and thickness were important parameters affecting the torsion behavior.

This study investigated the torsional behavior of HC-SCS columns using three-dimensional (3D) finite-element (FE) analysis. The FE models were validated with the experimental results of the six HC-SCS columns that were recently tested by Huang et al. (2013). The validated FE models were used to analyze and better understand the behavior of HC-SCS columns under pure torsion. An extensive parametric study was conducted to investigate important parameters that affect the torsional behavior of the HC-SCS columns. The parametric study included wider ranges of diameter-to-thickness ratios of both steel tubes, yield strength of the outer and inner steel tubes, the cylindrical unconfined

compressive strength of the concrete (f'_c), the existence of a concrete shell or inner steel tube, the height-to-diameter ratio of the column, and concrete shell thickness. Furthermore, simple design equations to calculate the torsion strength of HC-SCS column are proposed.

FE Modeling

Geometry

A total of six columns, namely CO111, CO112, CO211, CO212, CO311, and CO312, were tested by Huang et al. (2013). Each column had a height (H) of 550 mm (21.6 in.) and an outer steel tube diameter (D) of 165 mm (6.5 in.) (Figs. 1 and 2). The thickness of the outer steel tube (t_o) varied from 3.0 to 4.6 mm (0.12 to 0.18 in.). The inner steel tube's diameter (d) was either 42 mm (1.7 in.) or 75 mm (2.9 in.) with a thickness (t_i) that varied from 3.0 to 5.0 mm (0.12 to 0.20 in.). Hence, the concrete shell thickness ranged from 40.4 to 58.5 mm (1.60 to 2.30 in.). Two steel plates with dimensions of $235 \times 235 \times 25$ mm ($9.25 \times 9.25 \times 0.98$ in.) were attached to the column's top and bottom surfaces. The bottom steel plate of each column was fixed to the column on one side and to the ground on the other side. The top plate was connected to the column from one surface and to a loading plate from the other surface. The loading plate was $94 \times 324 \times 25$ mm ($3.7 \times 12.76 \times 0.98$ in.) (Fig. 1). Hence, the specimens examined in this study were tested as cantilever columns under pure torsion that were fixed to their footings. All
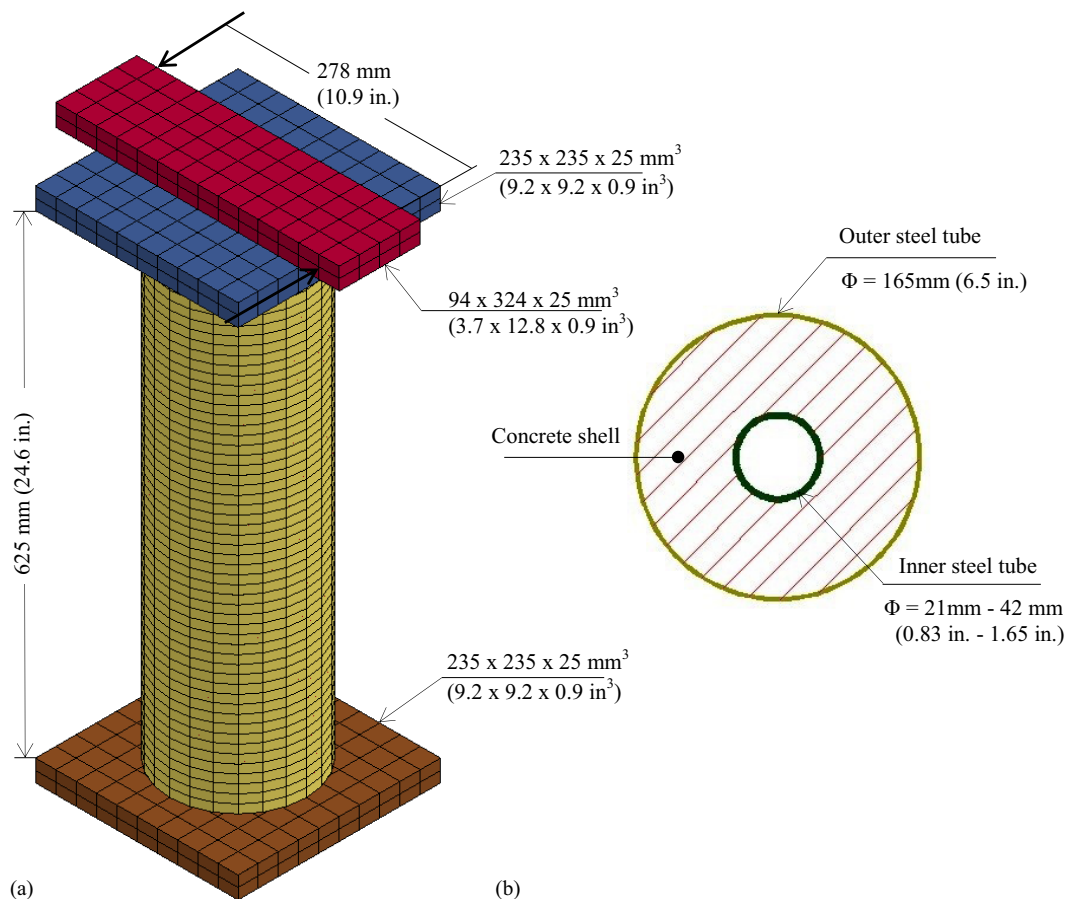

Fig. 1. (a) FE model of HC-SCS column; (b) cross-section view of HC-SCS column

of the columns were symmetric around the *X*- and *Y*-axes, and the rotational displacement was applied using the loading plate around the *Z*-axis. Table 1 summarizes the columns' variables.

A sensitivity analysis was performed to identify dimensions of the elements that would result in a good balance between the accuracy of the solution and the solution time. Each column's concrete core, steel top and bottom plates, and loading plate were modeled using 8-node brick solid elements. The concrete element had an average size of $8.75 \times 15 \times 10$ mm ($0.3 \times 0.6 \times 0.4$ in.). The element's steel plates and loading plate had an average size of $23.5 \times 23.5 \times 12.5$ mm ($0.9 \times 0.9 \times 0.5$ in.). Steel tubes were simulated using 4-node shell elements. A typical element's outer steel tube was 21.6×10 mm (0.8×0.4 in.). The typical element's inner steel tube was 7.8×10 mm (0.3×0.4 in.). Each FE model had 11,072 elements and 13,047 nodes.

To reduce the analysis time, all the solid elements of the column were modeled with constant stress and one-point quadrature integration. An hourglass control was used to prevent spurious singular modes in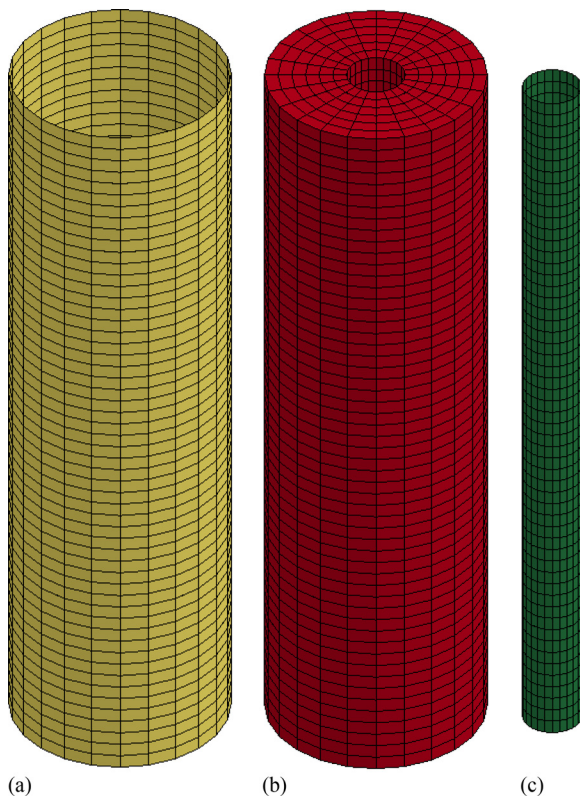 the elements. The hourglass value for all of the models was considered as the default value of 0.10 (Abdelkarim and ElGawady 2014b).

Material Models

Concrete

Various material models are available in *LS-DYNA* to simulate the concrete material. The Karagozian and Case Concrete Damage Model Release 3 (K&C model) was used in the current study because it was successfully used for similar applications and yielded good predictions of the performance of the investigated structural elements (Abdelkarim and ElGawady 2014b, 2016; Ryu et al. 2014; Youssf et al. 2014). The K&C model is a three invariant model that is built on the theory of plasticity with three shear failure surfaces: yield, maximum, and residual (Malvar et al. 1997).

The model adopts a shear dilation parameter (ω), which determines the appropriate plastic volumetric strain and, hence, can take into consideration the confinement effects. The shear dilation parameter is the fraction associativity defined as the initial ratio of the plastic volumetric strain increment that would occur if the plastic flow was fully associated in the hydrostatic plane. A default value of 0.5 was used in the current study for ω. A similar value was used in the literature for fiber reinforced polymer (FRP) confined concrete (Youssf et al. 2014). The concrete cylindrical compressive strength f_c' was 42 MPa (6,090 psi) for all of the columns. In the K&C model, the yield and failure surfaces' parameters are automatically generated with the input of f_c'. The K&C model uses automatic generation capabilities, given f_c' and ω as well as the equation of state, shown here as Eq. (1), to calculate the pressure as a function of current and previous volumetric strain. Once the pressure is known, the stress tensor can be calculated as being a point of a moveable surface that can be a yield surface or a failure surface (Noble et al. 2005; Crawford and Malvar 2006).

$$K = \frac{E_c}{3(1 - 2\upsilon)} \quad (1)$$

where υ is Poisson's ratio; and E_c is the elastic modulus, taken as 0.2 and 57,000 $\sqrt{f_c'}$ (ACI 2014) in this study, respectively.

The defined tensile stress-strain relationship in the material model is linear until the stress reaches the concrete modulus of rupture f_t. Beyond the f_t, the parameter η is used to gradually decrease the tensile stresses from f_t to zero in a smooth fashion while increasing the tensile strain. This is done by checking the equation of state subroutine.

Steel Tube

An elastoplastic material model 003-plastic_kinematic was used to describe the steel tube's stress-strain curve. The main parameters that were needed to describe this material model are the yield stress (f_y), elastic modulus (E), and Poisson's ratio (ν). For all of the models in this manuscript, f_y varied from 260 MPa (37,710 psi) to

Fig. 2. The FE model components: (a) outer steel tube; (b) concrete shell; (c) inner steel tube

Table 1. Summary of Column Variables (Data from Huang et al. 2013)

| Specimen label | Outer tube | | Inner tube | | f_{yo} [MPa (psi)] | f_{yi} [MPa (psi)] | f_{cu} [MPa (psi)] |
	D [mm (in.)]	t_o [mm (in.)]	d [mm (in.)]	t_i [mm (in.)]			
CO111	165 (6.5)	3.0 (0.12)	42 (1.65)	3.0 (0.12)	260.0 (37,700)	326.6 (47,357)	50 (7,250)
CO112		3.0 (0.12)	75 (2.95)	5.0 (0.20)	260.0 (37,700)	355.4 (51,533)	
CO211		4.0 (0.16)	42 (1.65)	3.0 (0.12)	286.4 (41,528)	326.6 (47,357)	
CO212		4.0 (0.16)	75 (2.95)	5.0 (0.20)	286.4 (41,528)	355.4 (51,533)	
CO311		4.6 (0.18)	42 (1.65)	3.0 (0.12)	365.6 (53,012)	326.6 (47,357)	
CO312		4.6 (0.18)	75 (2.95)	5.0 (0.20)	365.6 (53,012)	355.4 (51,533)	

Table 2. Summary of Experimental, FE, and Analytical Results

Column	T_{ue} [KN·m (k-ft)]	$T_{FE,0.01}$ [KN·m (k-ft)]	T_a [KN·m (k-ft)]	Error in $T_{FE,0.01}$ (%)[a]	Error in T_a (%)[a]	θ, experimental (°)	θ, FE (°)	Error in θ (%)
CO111	24.6 (18.1)	26.0 (19.2)	22.8 (16.8)	5.4	7.3	2.7	2.7	0
CO112	33.2 (24.5)	34.5 (25.4)	28.8 (21.2)	3.9	13.2	2.7	3.2	18
CO211	32.3 (23.8)	35.6 (26.3)	29.2 (22.9)	10.2	3.7	3.1	3.0	3
CO212	42.1 (31.1)	44.3 (32.7)	37.1 (27.4)	5.2	11.8	3.4	4.3	26
CO311	48.8 (36.0)	47.5 (35.0)	43.4 (32)	2.6	11.0	3.8	3.7	3
CO312	54.3 (40.0)	53.6 (39.5)	49.3 (36.4)	1.3	9.2	3.5	3.5	0

[a]The percentage of the absolute value of the difference between the experimental and the FE/analytical torque capacities divided by the experimental torque capacity.

365.4 MPa (52,997 psi), E was taken as 200 GPa (29,000, ksi), and ν was taken as 0.3. The steel tube's ultimate strain was considered as 0.04 (Abdelkarim and ElGawady 2014a). Once a steel element ruptured, either in shear or axial tension, it was removed from the model using the erosion feature in *LS-DYNA* to ensure the mode of failure. Under torsion loading, shear forces were exerted on the column resulting in tensile and compressive principle stresses. Hence, the erosion parameter was used to capture the rupture of the steel elements.

Steel Plates and Loading Plate

During the experimental work, no damage was observed in any of the top, bottom, or loading plates; hence, all three plates were modeled using the linear elastic material model. This material model was defined using a value of 200 GPa (29,000 ksi) for the steel elastic modulus (E) and 0.3 for the Poisson's ratio.

Concrete-Steel Interfaces

A surface-to-surface contact element was used to represent the interface between the steel tubes and concrete shell. This contact element considers slip and separation between the slave and master segments. This contact shows any slip/separation that occurs between the contact surfaces. The concrete shell and steel plates were contacted by node-to-surface contact. Node-to-surface contact acts similar to surface-to-surface contact. However, the slave node is allowed to penetrate on the master segment. A friction coefficient of 0.6 (Youssf et al. 2015) was assumed between the different elements that were in contact based on the sensitivity analysis and previous studies.

The steel tubes were fixed to the top and bottom steel plates during the experimental work. Hence, tied node-to-surface contact elements were used to bond the top and bottom steel plates to the column's top and bottom surfaces to simulate the full fixation during the experimental work. For the same reason, the loading plate was fully contacted to the top surface of the top steel plate using tied surface-to-surface contact elements. Because the concrete was enclosed between two steel tubes, the loss of moisture from the concrete was presented. The shrinkage effects were minimal and can be neglected.

Loading and Boundary Conditions

The displacement and rotation degrees of freedom were restrained at the bottom of the steel plate to simulate a fixation similar to what was used during the experimental work. The top of the loading plate was directionally restrained in the Z-direction to simulate the restraint from the hydraulic jacks used during the experiment. During the experimental work, the torque was applied at two equal displacements in opposite directions at the ends of the top loading plate with an arm length of 278 mm (2.3 in.), as shown in Fig. 1. The torque was applied to the column until the jack reached its maximum travel stroke. The experimental work was truncated before failure of the columns due to the stroke limitation of the hydraulic jacks. A similar loading procedure was used during the FE. However, the columns in FE were subjected to the torque until the columns failed in the form of either steel tube rupture or concrete shell failure.

Results and Discussions

Huang et al. (2013) defined the torque corresponding to a maximum shear strain in the outer steel tube of 0.01 ($\gamma_{os,0.01}$) as the torsion strength ($T_{FE,\,0.01}$) of the investigated columns. Beyond that shear strain, the increase in the torque was quite small and can be ignored for practical applications (Huang et al. 2013).

In the current FE study, two values of the torque were determined: the torsion strength obtained using the FE at $\gamma_{os,0.01}$ ($T_{FE,\,0.01}$) and the ultimate torsion at failure of the columns ($T_{FE,\,u}$). Table 2 summarizes the experimental torsion strength (T_{ue}) reported by Huang et al. (2013). Table 2 also presents $T_{FE,\,0.01}$. Furthermore, Fig. 3 shows the torque versus the twist for all of the columns based on the experimental and FE results. The twist was calculated at the top of the column.

As shown in the table and figure the values of T_{ue} and $T_{FE,0.01}$ were in a good agreement with the FE. The FE overpredicted the strength of four columns and underpredicted the strength of two columns. The error values ranged from 1.3 to 10.2% and were calculated as the absolute value of the difference between the experimental and the FE results divided by the experimental results. Furthermore, the model was able to predict the twist at $\gamma_{os,0.01}$ with an average error of 10%.

General Behavior of the Columns

As shown in Fig. 3, all the columns behaved very similarly with elastoplastic behavior. This section details the performance of Column CO111 and briefly reports the results of the other columns. Before yielding of the outer steel tube, which occurred at a twist of approximately $1°$, the relationship between the torque and twist displayed slight gradual stiffness degradation and can be considered approximately linear. The stiffness degradation occurred when some of the concrete shell elements went beyond their ultimate tensile capacity leading to gradual stiffness degradation in the models.

The typical shear stress-shear strain relationship of two different concrete elements at the column's middle-height cross section in which failure occurred is shown in Fig. 4(a). The distribution of Von Mises stresses along the column height and at the middle-
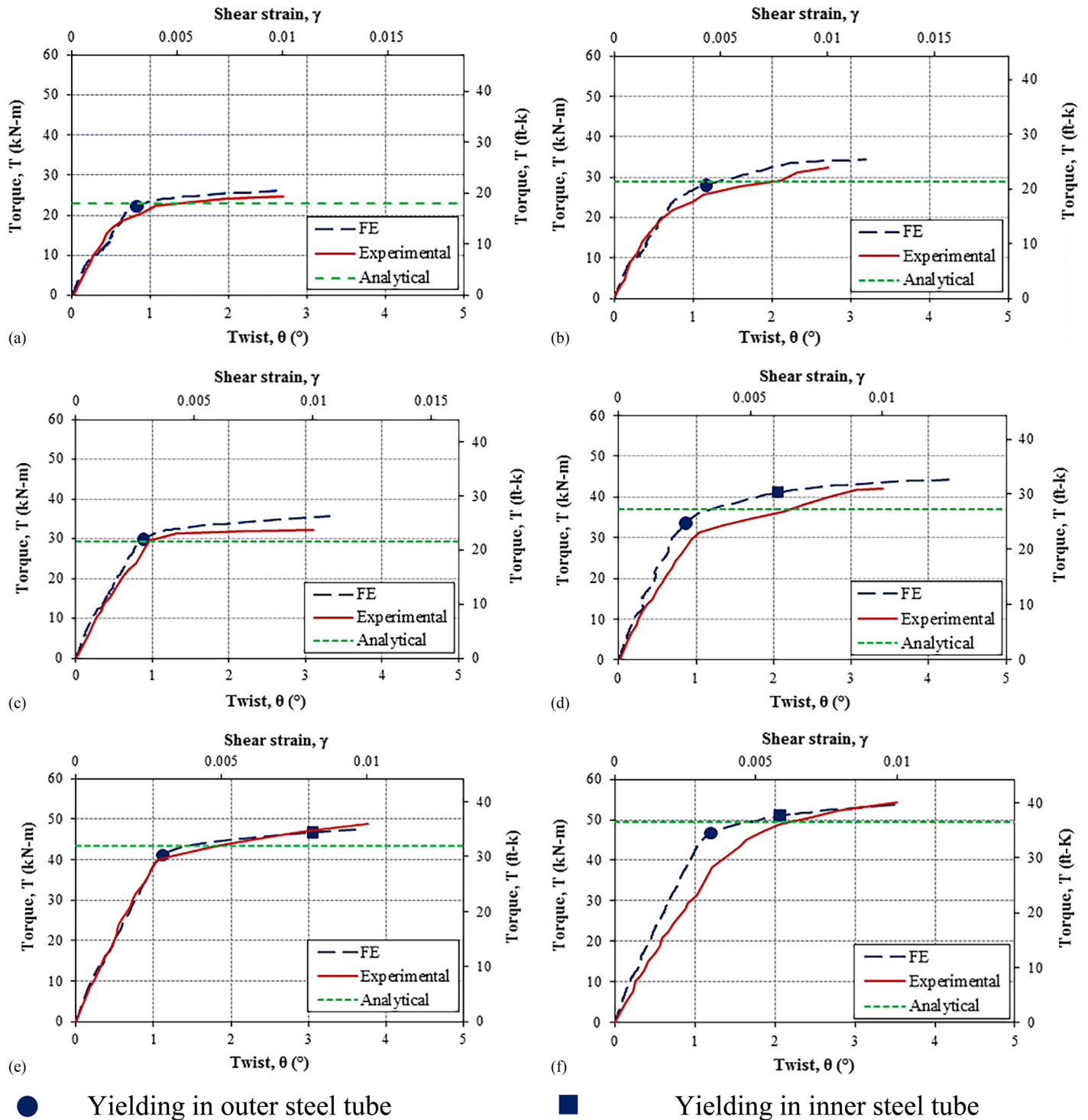
Fig. 3. Experimental (data from Huang et al. 2013) versus FE backbone curves for specimens: (a) CO111; (b) CO112; (c) CO211; (d) CO212; (e) CO311; (f) CO312

height cross section is also shown in Fig. 4(b). As shown in Fig. 4(b), there is a compressive stress concentration in the form of a spiral along the column height. Perpendicular to these compressive spirals, there is a limited tensile stress concentration [Fig. 4(b)]. As shown in Fig. 4, once the outer steel tube yielded, a greater shear strain demand was imposed on the concrete shell, leading to excessive principle tensile stresses. Beyond a shear strain value of 0.002, corresponding to a twist of 0.75°, the concrete element reached zero stiffness, indicating severe damage to the element.

Column CO111 reached $T_{FE,0.01}$ of 26.0 kN·m (19.2 kip-ft) during the FE analysis and 24.6 kN·m (18.1 kip-ft) during the experimental work [Fig. 3(a)]. The FE overestimated the strength of the column by 5.4%. The twist of the column at a shear strain of 0.01 in the steel was 2.7° for both the experimental work and FE analysis [Fig. 3(a)].

The experimental work was terminated at $\gamma_{os,0.01}$ due to the limitations on the hydraulic jack stroke, but the FE analysis was able to continue beyond this strain value. Fig. 5 shows the backbone curves
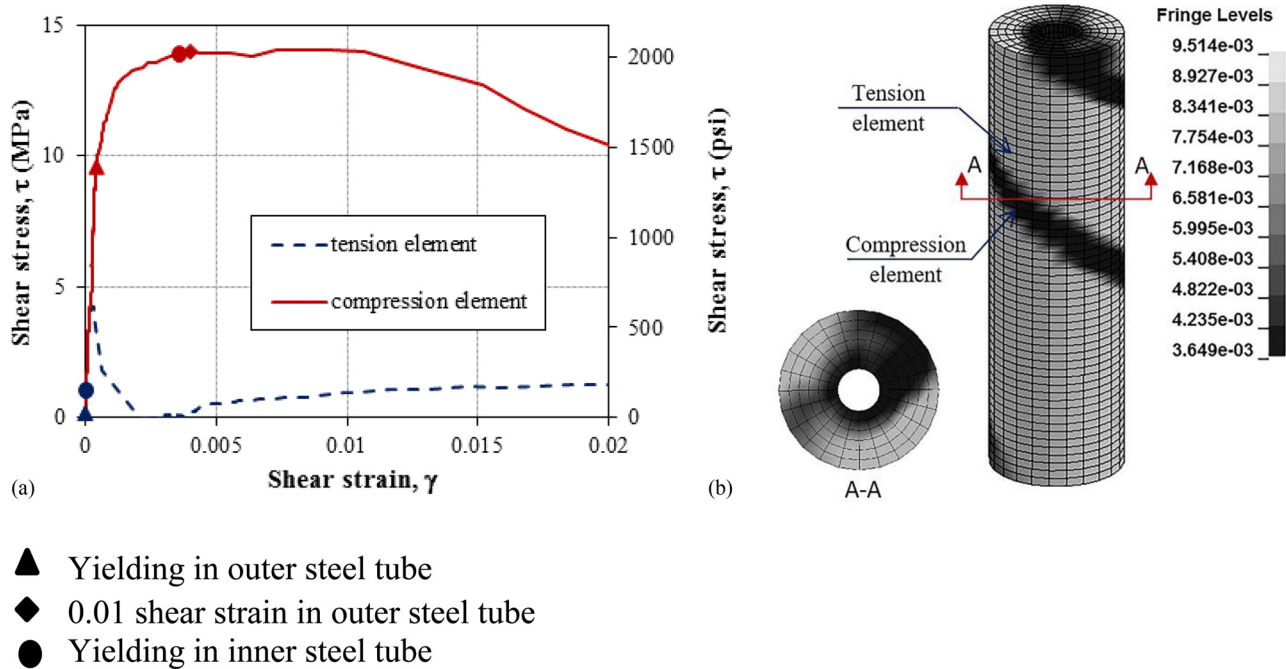
Fig. 4. (a) Typical shear stress-shear strain relationship of two concrete elements; (b) confined concrete shear stress at the initial shear crack for Column CO211 in GPa

for this set of columns until failure occurred. As shown in the figure, beyond $\gamma_{os,0.01}$, the twist at the top of the column increased considerably with a limited increase in the ultimate torsion. The increase in the ultimate torsion ranged from 17 to 28% compared with the $T_{FE, 0.01}$, whereas the twist increased by approximately 9.0 to 15.0 times the twist at a 0.01 shear strain in the steel. Beyond $\gamma_{os,0.01}$, the FE models showed that the concrete shell displayed significant cracking and dilation. Generally, the concrete dilation was not significant toward the inner direction compared with that toward the outer direction. The steel tubes from both the inner and outer direction countered the dilation. Increasing the applied twist caused the outer steel tube to yield resulting in a loss of confinement in the outer concrete shell. However, the existence of the inner steel tube constrained the concrete dilation toward the inner direction and decreased damage to the inner concrete shell. Fig. 4(a) shows the increase in the concrete compressive strength beyond γ of 0.014. Table 3 summarizes the shear stress of the outer steel tube at rupture and the ultimate torsion carried by the FE columns. The shear stress at failure was considered for the outer steel tube because it failed first.

Increasing the applied torque beyond the yielding of the outer steel tube caused significant stiffness softening to occur, leading to a significant increase in the twist with a minimal increase in the applied torque. This led to yielding of the inner steel tube at a twist ranging from 2 to 3°.

Fig. 6 shows a typical relationship between the shear stress versus the shear strain and the shear stress versus the twist for elements of the concrete, inner steel tube, and outer steel tube at the point of failure for column CO111. As shown in the figure, before the outer steel tube yielded, the outer steel tube's shear stress was more than triple that of the inner steel tube's shear stress indicting that the torsion strength is mainly provided by the outer steel tube. Furthermore, the inner steel tube's shear stress increased significantly after yielding took place in the outer tube. It should be noted that the inner steel tube yielded at higher stress compared with the

outer steel tube because both tubes have slightly different material characteristics, as show in Table 1 and reported by Huang et al. (2013). Once yielding occurred, each tube displayed strain hardening until failure. After the rupture of the outer steel tube, the torsion resistance of the column was reduced by about 70%. No vertical slip occurred between the concrete shell and steel tubes throughout the column's height due to the constraint imposed by the test setup.

Fig. 7 shows the column's failure mode obtained using the FE model. All of the six columns failed in a similar manner. The failure was triggered by a rupture in the outer steel tube in the helical direction at the middle height of each column. Failure of an element in *LS-DYNA* is indicated by removing the element using the erosion option, as explained earlier in this paper. Rupture occurred in several elements at the outer steel tube and resulted in a loss of confinement for the concrete in the outward direction; this resulted in an increase of concrete shell's volume in the outward direction, which caused the failure of the concrete shell. Finally, the inner steel tube alone carried the applied torque for a small imposed rotation after the concrete shell failed, leading to the abrupt rupture of the inner steel tube. The failure of the inner steel tube was abrupt due to the absence of the concrete shell that provided lateral stability. The outer steel tube ruptured in the helical direction at 390 mm (15.4 in.) from the column's bottom. The shear stress of the outer steel tube of Column CO111 at the failure was 191 MPa (27,702 psi). The concrete's maximum shear stress was considered when the initial small portion of the concrete elements failed prior to failure of the column. The ultimate torsion ($T_{FE, u}$) carried by Column CO111 before the failure was 33.3 kN·m (24.9 kip-ft) with an ultimate twist of 43.8°.

The torsion strength and twist of the columns at 0.01 shear strain in the steel during the FE study is summarized in Table 2 and displayed in Fig. 3. The ultimate torsion ($T_{FE, u}$) for the columns during the FE study is illustrated in Fig. 5. Fig. 8 shows the typical contribution of the steel tubes and concrete shell toward the torsion moment and the effect of confinement. The FE models showed that
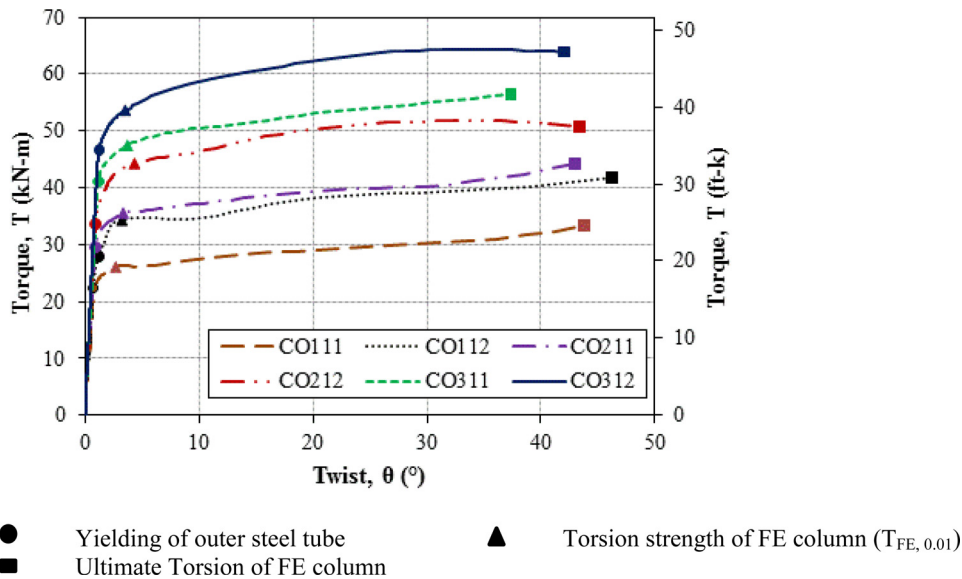
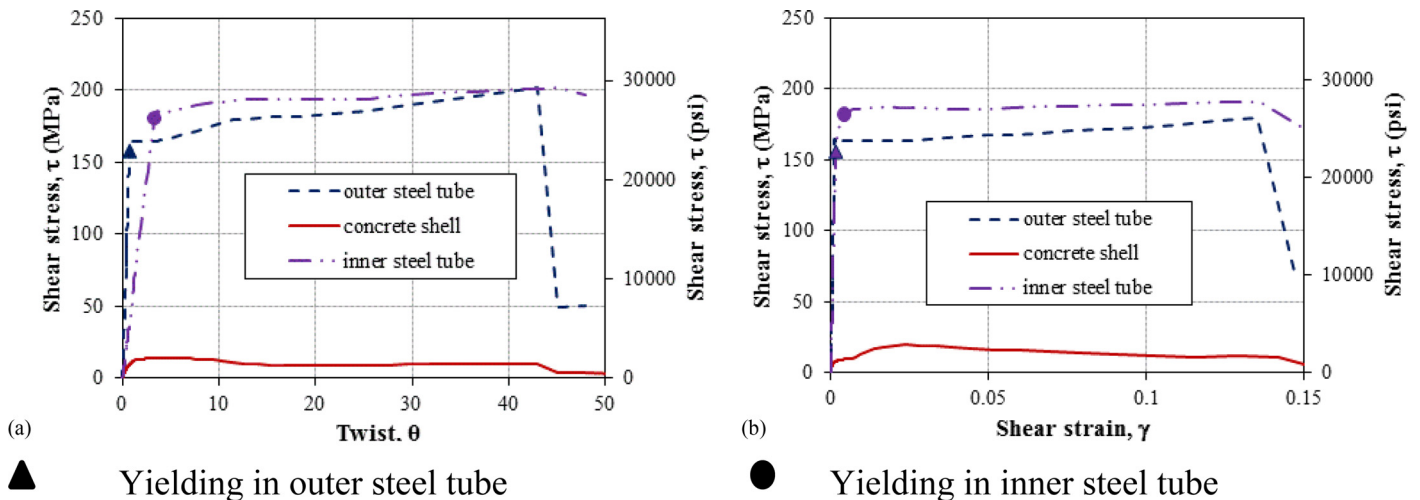**Fig. 5.** FE backbone cure for torque versus twist until failure

Fig. 6. Behavior of steel tubes and concrete shell at 550-mm (21.65-in.) height of Column CO211: (a) shear stress versus twist; (b) shear stress versus shear strain

columns CO112, CO211, CO212, CO311, and CO312 reached an FE torsion strength ($T_{0.01}$) of 34.5 kN·m (25.5 kip-ft), 35.6 kN·m (26.2 kip-ft), 44.3 kN·m (32.6 kip-ft), 47.5 kN·m (35.1 kip-ft), and 53.6 kN·m (39.50 kip-ft), respectively, compared with experimental torque values of kN·m (24.5 kip-ft), 32.3 kN·m (23.8 kip-ft), 42.1 kN·m (31.05 kip-ft), 48.8 kN·m (36.00 kip-ft), and 54.3 kN·m (40.0 kip-ft), respectively. The ultimate torsion ($T_{FE, u}$) of the FE columns (CO112, CO211, CO212, CO311, and CO312) ranged from 41.7 kN·m (30.8 kip-ft) to 63.9 kN·m (47.1 kip-ft). This represents an increase ranging from 15 to 20% over the corresponding $T_{0.01}$. The ultimate twists of the columns ranged from 38 to 47°, as shown in Fig. 5.

Parametric Study Analysis

A parametric study examined the influence of the main parameters of the column including the concrete's strength (f'_c), the outer steel

tube's strength (f_{yo}), the inner steel tube's strength (f_{yi}), the outer steel tube's diameter-to-thickness ratio (D/t_o), the concrete shell's thickness (t_c), the inner steel tube's diameter-to-thickness ratio (d/t_i), and the aspect ratio (H/D) on the torsional performance of HC-SCS columns.

Column CO112 was used as the reference column for this study with both steel tubes chosen to have identical yield strengths. Table 4 summarizes the parametric study variables and results. The modes of failure of the investigated columns were similar to those described before. Fig. 9 illustrates the torque-twist relationship of all the columns investigated in the parametric study. Fig. 10 illustrates the percentage change in the ultimate torsion of the HC-SCS column with respect to the change in parameters.

Yield Strength of Outer Steel Tube (f_{yo})

The outer steel tube's yield strength ranged from 310 to 586 MPa, and the ultimate strain was maintained at a constant

Table 3. Out Steel Tube Shear Stress and the Ultimate Torsion Moment at Failure

Column	Failure shear stress at out steel tube [MPa (psi)]	Ultimate torsion moment [KN·m (kip-ft)]
CO111	191 (27,702)	33.3 (24.5)
CO112	190 (27,557)	41.7 (30.7)
CO211	202 (29,297)	44.3 (32.6)
CO212	205 (29,732)	51.9 (38.2)
CO311	249 (36,114)	56.5 (41.6)
CO312	248 (35,969)	64.4 (47.5)

(a)   (b)   (c)
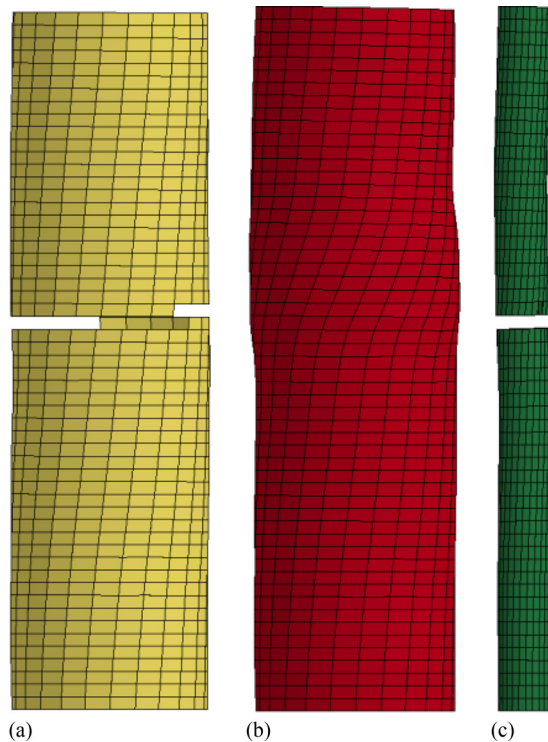
Fig. 7. Typical mode of failure of FE columns: (a) outer steel tube; (b) concrete shell; (c) inner steel tube

rate for all columns. Expectedly, the column's ultimate torsion increased linearly [Fig. 10(a)] as the outer steel tube's yield strength increased, because failures of these columns were triggered by the rupture of the outer steel tube [Fig. 9(a)]. The ultimate torsion increased by 45% when the yield strength of the outer steel tube increased by 86%. However, the ultimate twist of the column decreased by 13%.

Expectedly, the yield strength of the outer steel tube affects the behavior of the inner steel tube. As the yield strength of the outer steel tube increased, the contribution of the inner steel tube to the torsional resistance before the yielding of the outer tube decreased. However, the overall shear stress imposed on the inner steel tube before the failure of the column remained equal for different strengths of the outer steel tube. Gradual softening occurred in the columns' stiffness once the outer steel tubes yielded; this was followed by significant stiffness softening caused by yielding of the inner tubes. Increasing the outer steel tube's yield strength increased the columns' torque loads corresponding to yielding of the inner steel tubes, because yielding of these tubes occurred at approximately the
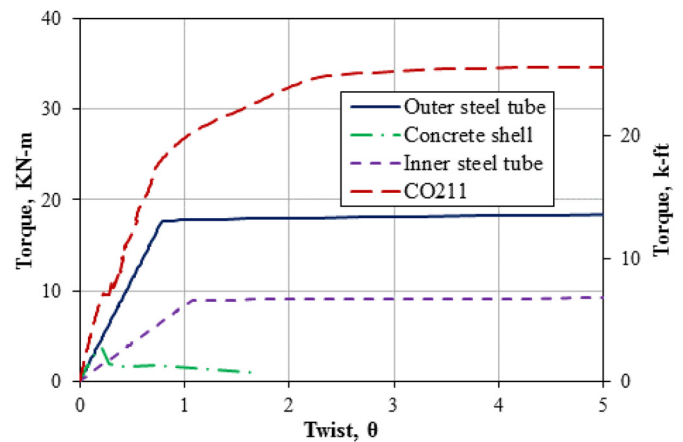

Fig. 8. Typical contribution of steel tubes and concrete shell toward torsion strength for Column CO112

Table 4. Summary of Parametric and Analytical Results

Parameter	Parametric value	FE, T_{FE}		Analytical, T_a	
		KN·m	k-ft	KN·m	k-ft
f_{yo}	310 MPa (45 ksi)	38.7	28.5	32.9	24.3
	380 MPa (55 ksi)	44.4	32.5	38.0	28.0
	448 MPa (65ksi)	47.2	34.8	42.2	31.1
	586 MPa (85 ksi)	53.7	39.6	53.0	39.1
f_{yi}	310 MPa (45 ksi)	42.4	31.2	36.4	26.8
	380 MPa (55 ksi)	44.4	32.7	38.0	28.0
	448 MPa (65ksi)	44.6	32.9	39.2	28.9
	586 MPa (85 ksi)	44.7	32.9	42.1	31.1
f_c'	10 MPa (1.5 ksi)	39.6	29.2	37.4	27.6
	40 MPa (5.8 ksi)	44.4	32.7	38.0	28.0
	70 MPa (10.2 ksi)	44.5	32.8	38.5	28.4
	100 MPa (14.5 ksi)	44.7	32.9	39.0	28.7
t_c	15 mm (0.6 in.)	61.3	45.2	58.9	43.4
	30 mm (1.2 in.)	49.7	36.6	48.3	35.6
	45 mm (1.8 in.)	44.4	32.7	38.0	28.0
	100 mm (2.9 in.)	35.3	26.0	35.0	25.8
D/t_o	15	107.0	79.0	111.5	82.3
	60	34.6	25.5	33.0	24.3
	120	26.4	19.5	22.9	16.9
	200	18.3	13.5	17.9	13.2
	250	16.9	12.5	16.3	12.1
d/t_i	15	44.4	32.7	38.0	28.0
	60	36.3	26.7	32.2	23.7
	120	35.0	25.8	31.1	22.9
	200	34.3	25.3	30.6	22.6
	250	33.9	25.0	30.5	22.5

same twist angle regardless of the outer steel tube's yield strength.

Yield Strength and Role of Inner Steel Tube (f_{yi})

The inner steel tube's strength was varied between 310 and 586 MPa, and the ultimate strain was maintained at a constant rate for all columns [Fig. 9(b)]. The inner steel tube's yield strength had little effect on the column's ultimate torsion. The column's ultimate torsion increased linearly by 16.5% when the inner steel tube's strength increased by 86% [Fig. 10(b)]. The removal of the inner

© ASCE

04016070-8

J. Bridge Eng.
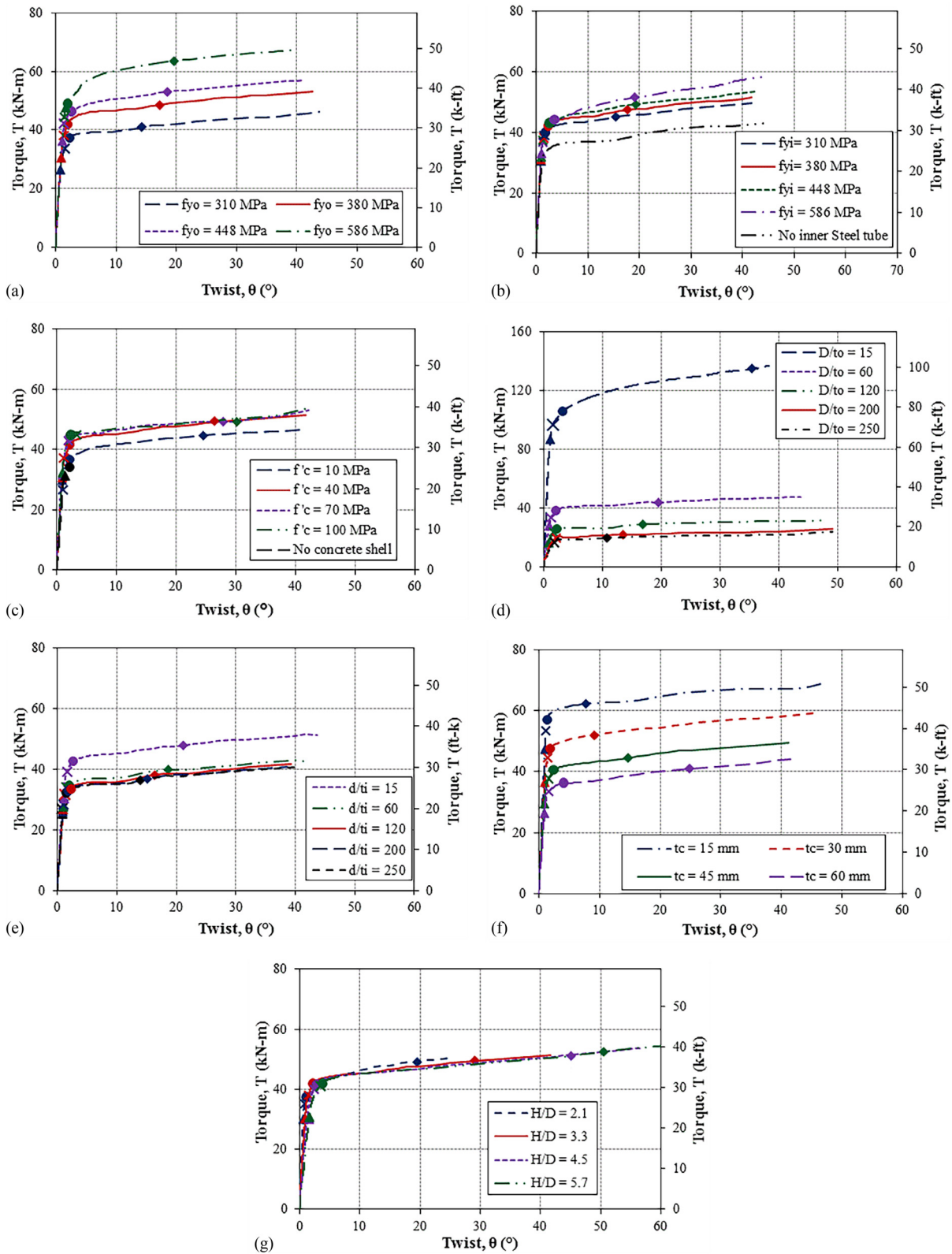
▲ Yielding in outer steel tube   ● Yielding in inner steel tube

X Compressive strength of concrete   ◆ Confined compressive strength of concrete

* The scale of the curve is different

Fig. 9. Effect of parameters on the torsional behavior of HC-SCS column
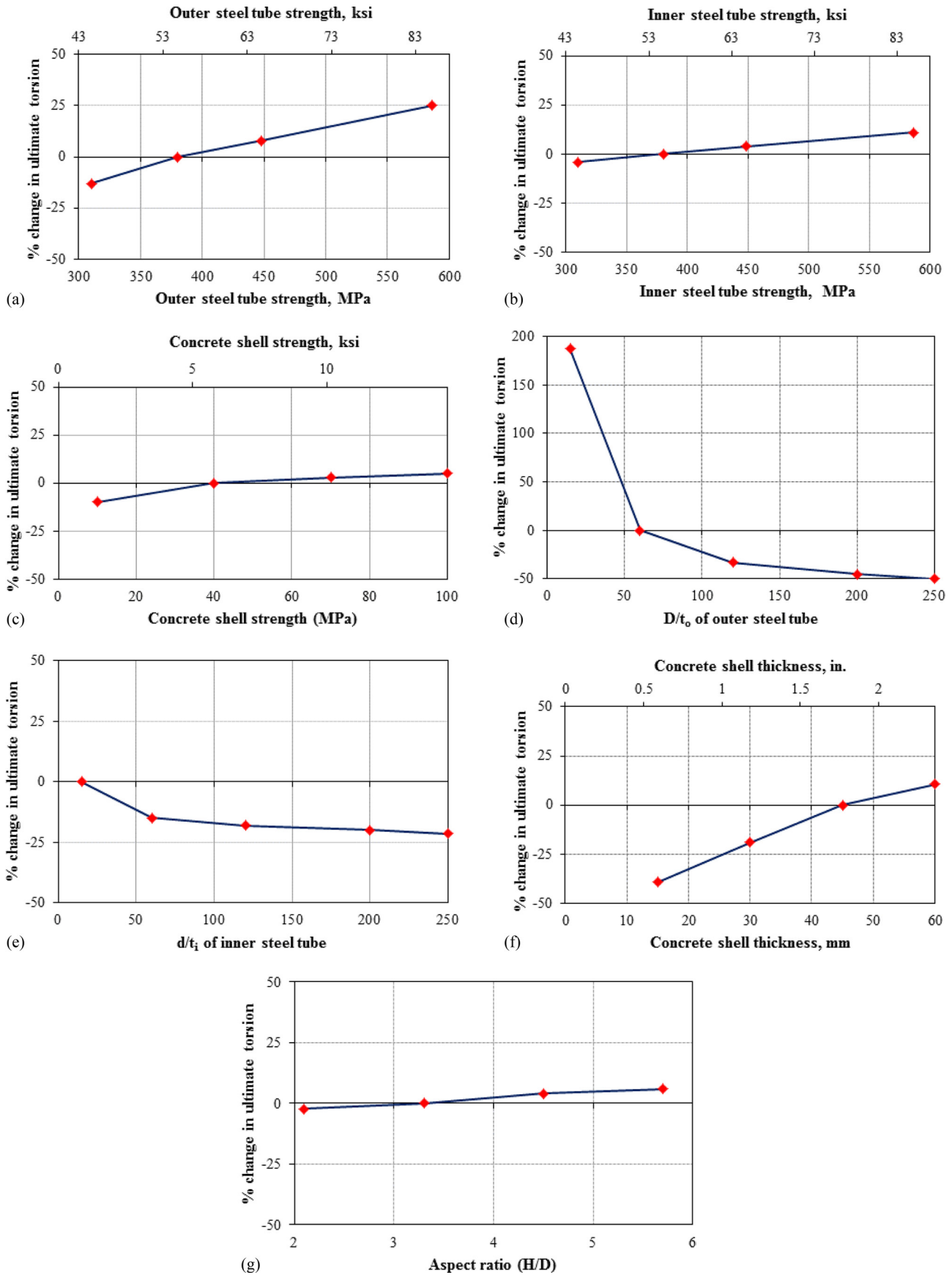
Fig. 10. Percentage change in ultimate torsion of HC-SCS column caused by change: (a) f_{yo}; (b) f_{yi}; (c) f_c'; (d) D/t_o; (e) d/t_i; (f) T_c; (g) H/D
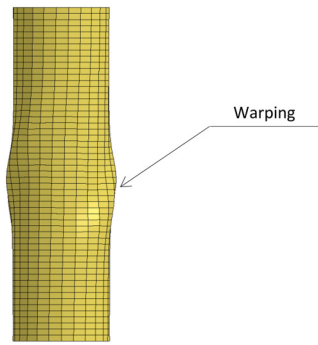
Fig. 11. Warping in outer steel tube

steel tube resulted in a 13% decrease in the column's ultimate torsion [Fig. 9(b)]. This decrease indicated that the inner steel tube's existence had a moderate effect on the column's torsional behavior. With the increase in the inner steel tube's strength, the ultimate twist was increased by 3.5%. Before yielding of the outer tube, the stress concentration on the outer steel tube was the same for all the columns. Beyond yielding of the outer tube, the column with the higher yield strength for the inner steel tube (i.e., 586 MPa) displayed a higher stiffness. After the outer steel tube yielded, most of the torsional load was carried by the inner steel tube. The stress concentration on the concrete shell was almost the same for all the columns. This resulted in no change in the behavior of the concrete shell with respect to the change in the inner steel tube's strength.

Compressive Strength (f'_c) and Role of Concrete

The concrete strength was varied between 10 and 100 MPa. Although the 10-MPa concrete may not be qualified as a candidate for structural applications in many codes and standards, it was used in this parametric study to investigate a wider range of parameters.

The ultimate torsion increased by 18% and the corresponding ultimate twist increased by 4% when the concrete strength increased by 90%. The torque-twist backbone curves are illustrated in Fig. 9(c). The backbone curves revealed that the concrete strength had less of an impact on the ultimate torsion compared with the ultimate twist. The outer steel tubes in all the columns yielded at the same twist angle, confirming the individual behavior of the steel tubes and concrete shell before yielding of the outer steel tube.

Before the outer steel tube yielded, there was a significant increase in the stiffness of the column with the increase in concrete strength. It was observed that the increase in ultimate torsion was caused by the initial stiffness of the concrete shell and the lateral stability provided by the concrete shell to the steel tubes. The concrete shell was removed in an additional column to observe the behavior of the column and the contribution of concrete shell in the capacity of the column [Fig. 9(c)]. The column's ultimate torsion decreased by 35% (with respect to $f'_c = 40$ MPa) without the presence of the concrete shell. This reduction in ultimate torsion occurred because the outer and inner steel tubes were not braced laterally, which was the concrete's effect. Therefore, the failure was warping in the outer steel tube with wall buckling, as shown in Fig. 11. Because the concrete was brittle in nature, the increase in its strength increased the brittle character of the column, as observed in the form of low twist with the increase in concrete strength.

D/t_o of Outer Steel Tube

The D/t_o of the outer steel tube was varied between 15 and 250 to study the stiffness and buckling behavior of the outer steel tube. The

change in the D/t_o was achieved by changing the thickness of the outer steel tube from 0.66 mm (0.03 in.) to 11 mm (0.43 in.). As shown in Fig. 9(d), the outer steel tube's D/t_o was one of the most influential parameters. The column's ultimate torsion decreased 5.7 times and its ultimate twist increased 1.32 times when the outer steel tube's D/t_o increased from 15 to 250 [Fig. 9(d)]. The effects of the change in the stiffness of the outer steel tube due to changing the D/t_o ratio were more prominent before yielding of the outer steel tube, as observed in the torque versus twist curve [Fig. 9(d)]. As explained earlier, strain hardening occurred in the outer steel tube after yielding, and most of the torsional load was carried by the inner steel tube. Hence, the effect of changing D/t_o after the yielding of the outer tube diminished. It is worth noting that the *AISC Manual* defines the critical local buckling of the empty steel tube at a diameter-to-thickness value of $0.07(E/f_y)$. This critical local buckling D/t_o for the investigated column was calculated as 36.8. The FE analyses showed no local buckling in the steel tubes even at a D/t_o value of 250, because of the lateral stability provided to the steel tube by the concrete shell.

The shear stress capacity of the concrete shell at the failure of the outer steel tube was decreased for the higher D/t_o ratio. This was caused by the concrete shell's decrease in confinement, which was provided by the outer steel tube. However, because the concrete shell's contribution to the ultimate torsion of the columns is relatively limited, this change in the confinement effect did not significantly change the strength of the columns. As mentioned previously, local buckling was not observed in any case. Hence, the shear stress carried by the inner and outer steel tubes at failure remained constant for different D/t_o ratios.

d/t_i of Inner Steel Tube

The d/t_i of the inner steel tube was varied between 15 and 250 to study the stiffness and buckling behavior of the inner steel tube. The d/t_i was changed by changing the thickness of the inner steel tube from 0.3 mm (0.01 in.) to 5 mm (0.2 in.). The inner steel tube d/t_i had little influence on the column's ultimate torsion. The column's ultimate torsion decreased by 20% and its ultimate twist decreased by 7% when the d/t_i of the inner steel tube increased 15.6 times [Fig. 9(e)]. Based on the above parametric study, the geometric term associated with the ultimate torsion is section modulus. For small diameters of the inner steel tube, with respect to the diameter of outer steel tube, the section modulus of the inner steel tube was not varied much with the altered d/t_i ratio. It resulted in a small change in the column's ultimate torsion for smaller diameters of the inner steel tube. As expected, the stiffness of the column was decreased with the increase in the inner steel tube's d/t_i ratio. The behaviors of the outer steel tube and the concrete shell were not altered with the inner steel tube's d/t_i ratio. The ultimate twist of the column was not significantly influenced, because the behavior of the column was mainly associated with the outer steel tube. The ultimate twist decreased with the increase in the inner steel tube's d/t_i ratio. The local buckling of the inner steel tube advanced with the increase in the d/t_i of the inner steel tube and inhibited the rotation of the column. However, the local buckling of the inner steel tube did not significantly affect the overall torsion behavior of the column.

Concrete Shell Thickness (T_c)

The concrete shell thickness had a major effect on the ultimate torsion of the column. The concrete shell thickness was varied from 15 mm (0.6 in.) to 60 mm (2.4 in.), representing 9.1 to 36.4% of the column's outer diameter. A constant diameter-to-thickness ratio of the inner steel tube was maintained by varying the thickness of the inner steel tube with the change in the concrete shell's thickness.
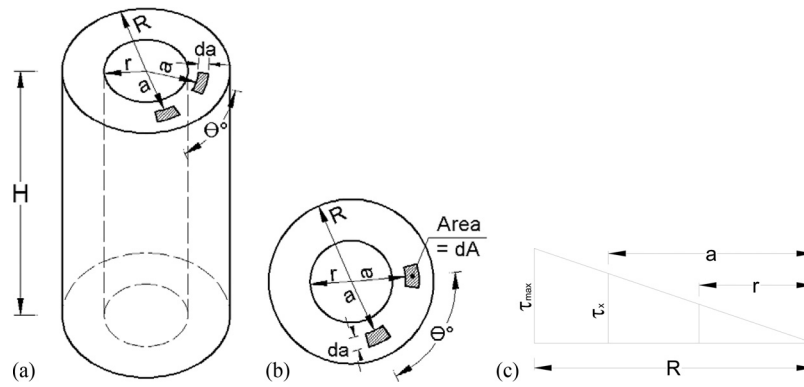
Fig. 12. Torsional terms on concrete shell: (a) isometric view; (b) cross-section view; (c) shear stress variation along the radius

Although the lower end in the investigated parameter may not reflect a practical application, it was used to obtain a thorough understanding of the effects of the concrete shell on the performance of HC-SCS columns.

As shown in Fig. 9(f), the column's ultimate torsion and ultimate twist decreased by 56 and 12%, respectively, with the increase in the concrete shell's thickness from 15 mm (0.6 in.) to 60 mm (2.4 in.). It should be noted that this decrease in strength is directly related to the reduction in the inner steel diameter and thickness, which companied the increase in the concrete shell thickness. For example, for a column with a concrete wall thickness of 15 mm (0.6 in.), both the inner and outer steel tubes reached yielding at almost the same torsional angle. For a column with a concrete wall thickness of 60 mm (2.4 in.), the inner steel tube reached to approximately half of the yield strength when the outer steel tube reached its yield strength. This indicated that the increase in the concrete shell's thickness reduced the demand on the inner steel tube. Furthermore, for a smaller concrete shell thickness [i.e., 15 mm (0.125 in.)], both steel tubes failed at the same twist. For a larger concrete shell thickness [i.e., 60 mm (2.4 in.)], the outer steel tube failed first and was followed by the rupture of the inner steel tube.

Aspect Ratio of Column (H/D)

The H/D ratio has very little influence on the column's ultimate torsion but has much influence on the ultimate twist. The H/D ratio was varied between 2.1 and 5.7. The column's ultimate torsion increased by 10%, and its ultimate twist increased by 210% when the column's aspect ratio increased by 170% [Fig. 9(g)]. Fig. 9(g) shows that the ultimate torsion of the columns remained approximately constant for different H/D ratios, because the ultimate torsion depends mainly on the material and cross-sectional characteristics of the columns. However, after yielding of the outer tubes, the column with the higher H/D ratio displayed significant stiffness softening, resulting in a significant increase in the ultimate twist at failure [Fig. 9(g)]. The column's mode of failure was outer steel tube rupture, as in previous parameters. The increase in the aspect ratio resulted in slenderness of the column, and it became less susceptible toward the applied torsional load.

Analytical Model

In this section, a simple analytical model to calculate the torsion strength of HC-SCS columns is developed and presented. The results of the parametric study (Fig. 9) showed that the inner and outer steel tubes of all specimens reached the yield strain at very

close twist angles. Moreover, the concrete shell also reached its unconfined compressive strength at twist angles close to those of the yielding steel tubes. Hence, the analytical torque capacity (T_a) of the HC-SCS columns can be calculated as the sum of three components: the capacity of the outer steel tube (T_{os}), the concrete shell (T_c), and the inner steel tube (T_{is}) as per Eq. (2).The error mainly resulted from the fact that the proposed model ignores the steel-hardening rule in calculating the torsion strength. The change in the diameter-to-thickness ratio and the yield strength of the inner steel tube does not endeavor the column's torsion strength significantly. Therefore, confinement to the concrete shell was considered only from the outer steel tube and was neglected from the inner steel tube.

$$T_a = T_{os} + T_c + T_{is} \qquad (2)$$

The torsion strength of the concrete shell was calculated by selecting a segment with an area (dA) located at a radial distance of a on the top surface of the concrete shell (Fig. 12). The inner and outer radii of the concrete shell are, respectively, represented as r, and R. The height of the column is H.

The applied torque resulted in a twist of θ and shear strain of γ.

$$\text{The rotated arc length } dl = a*\theta = H*\gamma \qquad (3)$$

$$\text{from Eq. (3), } \gamma = \frac{a * \theta}{H} \qquad (4)$$

$$\text{Hooke's law states } \tau = G * \gamma \qquad (5)$$

$$\text{From the Eq. (5), Eq. (4) transforms to } \tau_x = \frac{G * a * \theta}{H} \qquad (6)$$

The shear modulus is G, and τ_x is the shear stress of the elementary concrete segment.

Eq. (6) shows that the shear stress has a linear relationship with the radius of the column (Fig. 12).

The elementary shear force (dF) over the segmental area (dA) was calculated as

$$dF = \tau_x dA \qquad (7)$$

The torsion strength of the concrete shell (T_c) was obtained by integrating the elementary shear force (dF) multiplied by the lever arm (a) over the entire cross-sectional area (A) of the concrete shell

$$T_c = \int_r^R dF * a = \int_r^R (\tau_x dA)a \qquad (8)$$

The application of a similar triangle rule for Fig. 12(c) was based on Eq. 6

$$\frac{a}{R} = \tau_x / \tau_{max} \qquad (9)$$

Upon substituting Eq. 6 into Eq. 5 and over integration

$$T_c = \frac{\tau_{max}}{R} J_{pc} \qquad (10)$$

where

$$J_{pc} = \frac{\Pi(R^4 - r^4)}{2} \qquad (11)$$

From the ACI (2014), the cracking shear strength (τ_{max}) of the concrete

$$\tau_{max} = 4\sqrt{f'_{cc}} \qquad (12)$$

The steel tubes provide confinement to the concrete shell, enhancing the compressive strength, known as confined compressive strength of concrete (f'_{cc}), which can be calculated following, the procedure developed by Lee et al. (2009).

Similarly, the torsion strengths of the outer (T_{os}) and inner (T_{is}) steel tubes can be calculated as follows:

$$T_{os} = \tau_{yo} \frac{J_{po}}{R_o} \qquad (13)$$

$$T_{is} = \tau_{yi} \frac{J_{pi}}{R_i} \qquad (14)$$

where τ_y, J_p, and R are the shear stress, polar moment of inertia, and diameter of the steel tubes, respectively. The subscript O is used for the outer tube, and i is used for the inner tube. The shear stress can be calculated as $f_y/\sqrt{3}$ (Tabor 2000).

The torque applied at the yield of the outer steel tube resulted in a twist (θy), where θ_y can be calculated using Eq. (15) based on Eq. (6). The shear strain at the yield of the outer steel tube was considered as γ_y

$$\theta_y = \frac{\gamma_y * H}{R} \qquad (15)$$

The results of the analytical model were compared with those from the experimental work in Table 2 and Fig. 3. As shown in the figure and table, the analytical model had an average error of 9.4% in predicting the column's torsion strength. The twist of the columns at γ_y was between 0.63 and 1.08°. The average error in predicting the twist of the column at γ_y with the FE results was 12%. The parametric results of FE and the analytical model are good in agreement (Table 4).

Summary and Conclusions

The *LS-DYNA* software was used to conduct a FE analysis of HC-SCS columns. The HC-SCS columns consisted of a concrete wall that was sandwiched between steel tubes. The FE analysis results were validated against experimental results available in the literature. The proposed model was able to predict the behavior of HC-SCS columns under pure torsion. The K&C model, with automatically generated parameters, produced good results for concrete modeling, including the modeling of high-strength concrete. A parametric analysis was conducted by assuming the parameters and observing their influence on the T-θ curves. Six parameters influenced the column's ultimate torsion. The outer steel tube's D/t_o ratio was the governing parameter that controlled the column's ultimate torsion followed by concrete shell thickness and then the strength of the outer steel tube. The aspect ratio (H/D) of the column and inner steel tube's strength had little influence on the column's ultimate torsion. All of the six columns had similar failure sequences. The only change in failure was the change along the height of the column. The simplified analytical model that was developed based on the parametric study was in good agreement with the experimental results.

Acknowledgments

Notation

The following symbols are used in this paper:

D = outer diameter of inner steel tube;
d = outer diameter of outer steel tube;
f_{cu} = characteristic 28-day concrete cube strength;
f_{yi} = yield strength of inner steel tube;
f_{yo} = yield strength of outer steel tube;
f'_c = unconfined compressive strength of concrete;
H = height of the column;
J_{pc} = polar moment of inertia of concrete;
J_{pi} = polar moment of inertia of inner steel tube;
J_{po} = polar moment of inertia of outer steel tube;
T_a = torsion strength predicted by simplified analytical model;
$T_{FE, u}$ = ultimate torsion at failure of FE column;
$T_{FE, 0.01}$ = torsion strength predicted by FEA model;
T_{ue} = experimental torsion strength;
t_i = thickness of inner steel tube;
t_o = thickness of outer steel tube;
θ_y = twist at yield of outer steel tube;
τ_c = shear stress of concrete;
τ_{yi} = shear stress of inner steel tube; and
τ_{yo} = shear stress of outer steel tube.

References

Abdelkarim, O., and ElGawady, M. (2014a). "Behavior of hybrid FRP-concrete-steel double-skin tubes subjected to cyclic axial compression." *Structures Congress 2014*, 1002–1013.

Abdelkarim, O., and ElGawady, M. (2014b). "Analytical and finite-element modeling of FRP-concrete-steel double-skin tubular columns." *J. Bridge Eng.*, 10.1061/(ASCE)BE.1943-5592.0000700, B4014005

Abdelkarim, O. I., and ElGawady, M. A. (2016). "Design of short reinforced concrete bridge columns under vehicle collision." *Transportation Research Record*, 2592, 27–37.

Abdelkarim, O., Gheni, A., Anumolu, S., and ElGawady, M. (2015). "Seismic behavior of hollow-core FRP-concrete-steel bridge columns." *Structures Congress 2015*, 585–596.

ACI (American Concrete Institute). (2014). "Building code requirements for structural concrete (ACI318-11) and commentary." *(318R-11)*, Farmington Hills, MI.

Beck, J., and Kiyomiya, O. (2003). "Fundamental pure torsion properties of concrete filled circular steel tubes." *J. Mater Conc. Struct. Pavements*, 85–96.

Belarbi, A., Suriya Prakash, S., and Silva, P. (2008). *"Flexure-shear-torsion interaction of RC bridge columns."* *Concrete Bridge Conference*, Federal Highway Administration, Washington, DC, Paper No. 6.

Bi, K., Hao, H., and Ren, W. X. (2013). "Seismic response of concrete filled steel tubular arch bridge to spatially varying ground motions including local site effect." *Adv. Struct. Eng.*, 16(10), 1799–1817.

Crawford, J. E., and Malvar, L. J. (2006). "User's and theoretical manual for K&C concrete model." *Rep. TR-06-19.1*, Karagozian and Case, Burbank, CA.

Dawood, H., ElGawady, M., and Hewes, J. (2011). "Behavior of segmental precast post-tensioned bridge piers under lateral loads." *J. Bridge Eng.*, 10.1061/(ASCE)BE.1943-5592.0000252, 735–746.

Dawood, H., ElGawady, M., and Hewes, J. (2014). "Factors affecting the seismic behavior of segmental precast bridge columns." *Front. Struct. Civ. Eng.*, 8(4), 388–398.

Dong, C. X., and Ho, J. C. M. (2012). "Uni-axial behaviour of normal-strength CFDST columns with external steel rings." *Steel Compos. Struct.*, 13(6), 587–606.

Elchalakani, M., Zhao, X. L., and Grzebieta, R. H. (2002). "Tests of concrete-filled double skin CHS composite stub columns." *Steel Compos. Struct.*, 13(6), 587–606.

Han, L. H., Huang, H., Tao, Z., and Zhao, X. L. (2006). "Concrete-filled double skin steel tubular (CFDST) beam–columns subjected to cyclic bending." *Eng. Struct.*, 28(12), 1698–1714.

Han, L. H., Yao, G. H., and Tao, Z. (2007). "Performance of concrete-filled thin-walled steel tubes under pure torsion." *Thin Walled Struct.*, 45(1), 24–36.

Hassanein, M. F., Kharoob, O. F., and Liang, Q. Q. (2013). "Circular concrete-filled double skin tubular short columns with external stainless steel tubes under axial compression." *Thin Walled Struct.*, 73, 252–263.

Huang, H., Han, L. H., and Zhao, X. (2013). "Investigation on concrete filled double skin steel tubes (CFDSTs) under pure torsion." *J. Constr. Steel Res.*, 90, 221–234.

Lee, E., Yun, B., Shim, H., Chang, K., and Lee, G. (2009). "Torsional behavior of concrete-filled circular steel tube columns." *J. Struct. Eng.*, 10.1061/(ASCE)0733-9445(2009)135:10(1250), 1250–1258.

Li, W., Han, L. H., and Chan, T. (2014). "Tensile behaviour of concrete-filled double-skin steel tubular members." *J. Constr. Steel Res.*, 99, 35–46.

Lin, M. L., and Tsai, K. C. (2001). "Behaviour of double-skinned composite steel tubular columns subjected to combined axial and flexural loads." *Proc., 1st International Conf. on the Steel and Composite Structures*, Techno-Press, Taejon, Korea, 1145–1152.

LS-DYNA 971 R3 [Computer software]. Livermore Software Technology, Livermore, CA.

Lu, H., Zhao, X., and Han, L. H. (2010). "Testing of self-consolidating concrete-filled double skin tubular stub columns exposed to fire." *J. Constr. Steel Res.*, 66(8–9), 1069–1080.

Malvar, L. J., Crawford, J. E., Wesevich, J. E., and Simons, D. (1997). "A plasticity concrete model for DYNA3D." *Int. J. Impact Eng.*, 19(9-10), 847–873.

Mondal, T. G., and Prakash, S. S. (2015a). "Effect of tension stiffening on the behaviour of reinforced concrete circular columns under torsion." *Eng. Struct.*, 92(1), 186–195.

Mondal, T. G., and Prakash, S. S. (2015b). "Nonlinear finite-element analysis of RC bridge columns under torsion with and without axial compression." *J. Bridge Eng.*, 10.1061/(ASCE)BE.1943-5592.0000798, 04015037.

Mullapudi, T. R. S., and Ayoub, A. (2012). "Analysis of reinforced concrete columns subjected to combined axial, flexural, shear and torsional loads." *J. Struct. Eng.*, 561–573.

Nie, J. G., Wang, Y. H., and Fan, J. S. (2012). "Experimental study on seismic behavior of concrete filled steel tube columns under pure torsion and compression–torsion cyclic load." *J. Constr. Steel Res.*, 79, 115–126.

Noble, C., Kokko, E., Darnell, I., Dunn, T., Hagler, L., and Leininger, L. (2005). "Concrete model descriptions and summary of benchmark studies for blast effects simulations." *Rep. No. UCRL-TR-215024*, Lawrence Livermore National Laboratory, Livermore, CA.

Prakash, S. S., and Belarbi, A. (2009). "Bending-shear-torsion interaction features of RC circular bridge columns—An experimental study." *SP265, Paper No. SP-2*, American Concrete Institute, Farmington Hills, MI.

Ruili, H., Sneed, L. H., and Belarbi, A. (2014). "Torsional repair of severely damaged column using carbon fiber-reinforced polymer." *ACI Struct. J.*, 111(3), 705–716.

Ryu, D., Wijeyewickrema, A., ElGawady, M., and Madurapperuma, M. (2014). "Effects of tendon spacing on in-plane behavior of post-tensioned masonry walls." *J. Struct. Eng.*, 10.1061/(ASCE)ST.1943-541X .0000849, 04013096.

Tabor, D. (2000). *Hardness of metals*, Clarendon Press, Oxford, U.K.

Tao, Z., and Han, L. H. (2006). "Behaviour of concrete-filled double skin rectangular steel tubular beam–columns." *J. Constr. Steel Res.*, 62(7), 631–646.

Tao, Z., Han, L. H., and Zhao, X. L. (2004). "Behaviour of concrete-filled double skin (CHS inner and CHS outer) steel tubular stub columns and beam-columns." *J. Constr. Steel Res.*, 60(8), 1129–1158.

Wei, S., Mau, S., Vipulanandan, C., and Mantrala, S. (1995). "Performance of new sandwich tube under axial loading: Experiment." *J. Struct. Eng.*, 10.1061/(ASCE)0733-9445(1995)121:12(1806), 1806–1814.

Youssf, O., ElGawady, M. A., Mills, J. E., and Ma, X. (2014). "Finite element modelling and dilation of FRP-confined concrete." *Eng. Struct.*, 79, 70–85.

Youssf, O., ElGawady, M. A., and Mills, J. E. (2015). "Displacement and plastic hinge length of FRP-confined circular reinforced concrete columns." *Eng. Struct.*, 101, 465–476.

Zhao, X. L., Han, B., and Grzebieta, R. H. (2002). "Plastic mechanism analysis of concrete-filled double-skin (SHS inner and SHS outer) stub columns." *Thin Walled Struct.*, 40(10), 815–833.

Zhao, X. L., Tong, L. W., and Wang, X. Y. (2010). "CFDST stub columns subjected to large deformation axial loading." *Eng. Struct.*, 32(3), 692–703.